A NEW WALL CURRENT MONITOR FOR THE CERN PROTON SYNCHROTRON

J.M. Belleman[*], W. Andreazza, CERN, Geneva, Switzerland
A.A. Nosych, ALBA-CELLS Synchrotron, Cerdanyola del Vallès, Spain

Abstract

Wall Current Monitors are the devices of choice to observe the instantaneous beam current in proton accelerators. These entirely passive transformers deliver a high-fidelity image of the beam intensity in a bandwidth spanning from about 100kHz up to several GHz. They serve as a signal source for a diverse set of applications including Low Level RF feedback and longitudinal diagnostics such as bunch shape measurements and phase-space tomography. They are appreciated for their excellent reliability, large bandwidth and unsurpassed dynamic range. We describe the design of a new Wall Current Monitor for the CERN Proton Synchrotron with a useful bandwidth of 100kHz to 4GHz. Two such devices have been installed in the PS machine and are now used in regular operation. Some usage examples will be shown.

THE CERN PROTON SYNCHROTRON

CERN's Proton Synchrotron is a 628 m circumference, 26 GeV accelerator operating since 1959. Over the years, it has served to accelerate protons and electrons and their anti-particles, as well as several ion species. Today it is an important part of the CERN injector complex, delivering both protons and lead ions to the Large Hadron Collider via the Super Proton Synchrotron, as well as serving many other clients with its dedicated experimental area.

WALL CURRENT MONITOR PRINCIPLE

As a beam of particles travels through a conducting vacuum tube, it is accompanied by an image charge of equal magnitude but opposite sign flowing along the inside wall of the tube [1]. This co-moving wave of charge constitutes a localised current. If we were to cut the vacuum tube and place an impedance across the gap, this current would develop a voltage which is an accurate replica of the beam current.

To confine signal currents to a well-defined geometry, the gap is surrounded by a conducting shell. In this design the gap is empty, so the shell also holds the vacuum. Inside the shell are ferrite toroid cores that increase the WCM inductance and thereby extend the lower cut-off frequency downwards (Fig. 1). The whole arrangement is basically a single-turn transformer with the beam in the role of the primary 'winding', the conducting shell and the inner chamber as the secondary and the ferrite toroids as the core (Fig. 2).

---

[*] jeroen.belleman@cern.ch
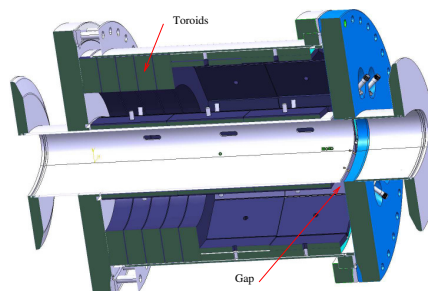
Figure 1: Cut-away view of the Wall Current Monitor.
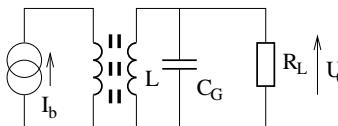
Figure 2: Simplified WCM equivalent circuit.

The WCM's low frequency cut-off is $\omega_L = \frac{R_L}{L}$, with L the inductance of the ferrite toroids and R_L the gap load resistance. The ferrite toroids are Ferroxcube T240/160/20-8C11, with a single-turn inductance of about $2\,\mu$H. Five toroids supply a total of about $10\,\mu$H. With the gap load resistance of $6\,\Omega$, this yields a lower cut-off frequency of about $100\,$kHz.

The inner surfaces of the shell, as well as the outer surface of the beam pipe, are covered in Ferroxcube 4S60 absorptive ferrite tiles. This does not contribute substantially to the transformer inductance, but it muffles the EM energy propagating into the space between the shell and the beam pipe, which would otherwise look like a coaxial shorted stub in parallel with the gap load resistance.

Despite the liberal use of absorptive ferrite, the high frequency response is dominated by various EM wave effects —cavity resonances— well before it finally drops off because of the gap capacitance C_G. A lower gap load resistance would widen the WCM's bandwidth at both ends of the frequency response, but reduce the output signal for a given beam intensity.

Since the ferrites are installed inside the vacuum, they were all subjected to chemical degreasing, followed by a bake-out at $1000\,°$C in air. The bake-out does not discernably affect the ferrite properties [1]. The main residual gas source was adsorbed water. Although the outgassing rate is not enormous, a WCM has a dedicated ion pump.
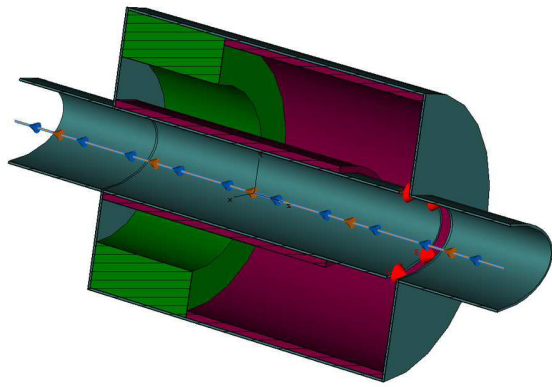
Figure 3: WCM simulation model.

SIMULATION

Simulation models were used to sort out WCM architecture variants. This also helped to decide on details of the WCM construction: whether or not to use oval-to-cylindrical transitions, how to position the feedthroughs, probe geometry, where to put absorbing ferrites, etc. We converged on the model shown in Fig. 3 as being best. Inductive ferrite is green, absorptive ferrite is bordeaux red and the gap loads are represented by the little bright red cones. To avoid burdening the model with details, some specific parts, such as the feedthroughs, were simulated separately.

To make the best of the high-frequency response, the gap is free of any dielectric material. Eight coaxial 50 Ω probes bridge the gap. Each of these probes is brought out via a vacuum-tight controlled-impedance feedthrough (Fig. 4) with an SMA connector on the outside. The feedthroughs are made by Times Microwave Systems from an original Fermilab design.
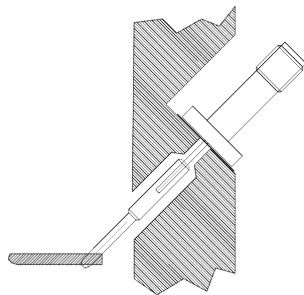
Figure 4: Probe and feedthrough geometry.

The cross-section of the CERN Proton Synchrotron vacuum chamber is oval and the distribution of the image current is therefore not homogeneous, even for a perfectly centred beam. The probes are spaced to sit at equal angular distances seen from the central axis (Fig. 5). Each thus collects a similar fraction of the image current for a centred beam. The eight partial outputs are then combined into one on the outside of the WCM.
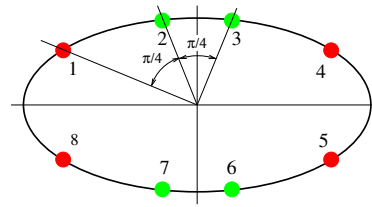
Figure 5: Distribution of probe positions around the gap perimeter.

COMBINERS

A tree of elementary passive star combiners merges the eight outputs of the wall current monitor into two identical, approximately position-independent, output signals (Fig. 6) [2, 3]. Matched-length 50 Ω coax cables are used for the interconnections. The blocks marked 'T' are coaxial terminators. Attenuators serve to spread-out signal power to prevent overload damage, or to enhance the damping of transients. The attenuators are rated for 15 W average. The *peak* power in each individual attenuator approaches 2 kW for the most intense beams, albeit fortunately at tiny dutycycles.
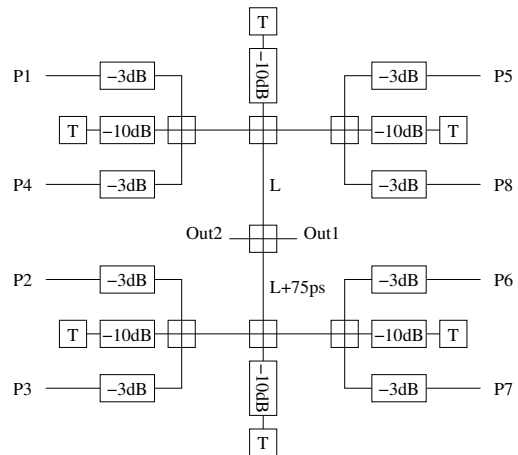
Figure 6: Combiner tree.

Each elementary star combiner is a simple junction of four coaxial transmission lines (Fig. 7). Seven are needed for a complete tree. Despite their apparent simplicity, these devices have some subtleties in their behaviour. Let's consider the case of a simple four-port combiner:

Figure 7: An elementary four-port star combiner.

As shown in Fig. 8, suppose all ports are terminated in their characteristic impedance Z_0. Ideally, two identical input signals travel from the sources towards the junction, are superimposed with the resultant sum divided over the two outputs. In practice, the input signals may not be exactly equal and the source impedances aren't necessarily equal to Z_0, nor even the same.
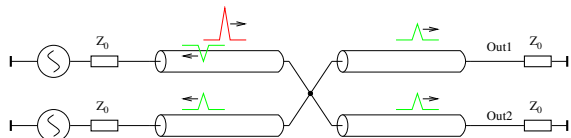
Figure 8: Model of an elementary four-port star combiner.

A signal propagating on a transmission line with impedance Z_0 reflects on a discontinuity with impedance Z according to:

$$\Gamma = \frac{Z - Z_0}{Z + Z_0} \qquad (1)$$

From the point of view of a single signal incident on the junction (red in Fig. 8), $Z = \frac{Z_0}{3}$, so there is a reflection of $\Gamma = -\frac{1}{2}$ of the incident signal travelling back to its source, while $+\frac{1}{2}$ travels towards each of the three other ports (green in Fig. 8). If we have two identical incident signals, the reflection of each is exactly cancelled by the forward travelling contribution from the other input, and all energy ends up in the output loads on the right.

If the two incident signals are *not* equal, half of the difference is reflected back to each of the inputs. Now, if the source impedances are equal to Z_0, these reflections are absorbed and we're done. If the source impedances are the same but *not* equal to Z_0, new reflections depart once more towards the junction. These reflections are exactly complementary, so at the junction they cancel and nothing shows up in the outputs. All energy is returned once more to the sources. This repeats until all energy is dissipated in the source impedances.

If the source impedances are *not* equal, the secondary reflections do not cancel when they reach the junction again and some energy *does* end up in the output. This then repeats until all energy is dissipated, this time in both the source impedances and the output loads. This latter situation yields an exponentially decaying tail of afterpulses, piling up into a single trailing messy transient. Clearly this is a very undesirable result.

For a WCM in a cylindrical vacuum pipe, it's easy to make sure that all ports have the same source impedance. However, the PS has an oval chamber, as does this WCM. Even for a perfectly centred beam, it has two sets of outputs with different output signals and different source impedances.

For off-centre beams, the signal levels will differ even within one set. Measurements have shown that the return loss of the WCM ports is in the range of 5 to 10 dB. Signal energy bouncing back and forth between the ports will be damped relatively slowly. It is therefore beneficial to add attenuators between the ports and the combiners. This reduces the mismatch between ports and provides a faster means of dissipating multiple reflections. The WCM fortunately provides enough signal to make this acceptable.

LAB TEST SETUP

In this section, rather than showing smooth progress from concept to result, we choose to expose some of the nitty-gritty laboratory work.

To simulate the passage of a beam in the lab, the WCM is mounted between a pair of short pieces of standard PS vacuum pipe and a $\oslash$ 6 mm rod is strung through the centre, thus forming a coaxial line. A pulse generator injects signals onto this line (Fig. 9). The rod's characteristic impedance is $160\,\Omega$. It is important that the rod present the smoothest impedance possible. Any discontinuity causes reflections, complicating the interpretation of measurements and placing additional uncertainties on the current flowing on the line.
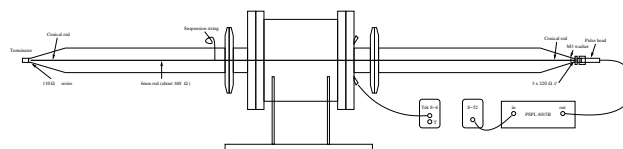
Figure 9: Lab test setup.

We went to considerable effort to smooth out any impedance variations. To keep the rod from sagging under its own weight, it was suspended near the centre with a simple piece of string. Padding resistors match both ends of the rod to $50\,\Omega$. This is a great opportunity to discover that resistors are not just resistive, and that different resistors have different parasitic capacitances and inductances. For example, low-value 1206 SMD chip resistors are predominantly capacitive at high frequency, whereas 1206 MELF resistors are inductive. We used MELFs, combined with capacitive shims to tune out the inductance. The first and last few decimeters of the chamber and the rod are constant-ratio cones, narrowing down from the full size pipe to diameters compatible with standard N-connectors.

The vacuum flanges at each end of the WCM resonate at 2.5 GHz. This was reduced by inserting RF springs in the gaps between the flanges.

Some residual reflections cannot be avoided. The time-domain reflection plot of Fig. 10 shows what could finally be achieved. The vertical scale is normalised to the incident step. The tallest reflections are about 4 %.
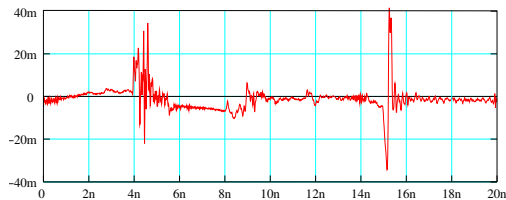
Figure 10: Beam simulation rod TDR plot.

The reflections around 4 ns and 15 ns in Fig. 10 are from the ends of the rod. The small reflections at 8 ns and 12 ns are the vacuum flanges at either end of the WCM. The step at 9 ns is the gap of the WCM itself. These measurements were taken using a Tektronix S-52 pulse generator and an S-6 sampler, having a 30 ps risetime, or equivalently a 10 GHz bandwidth.

Despite the effort invested in simulating the main structure of the WCM, several surprises cropped up, resulting from seemingly innocent mechanical details. For example, the absorbing ferrites along the outside wall are mounted on two aluminium hoops that are held in place by a narrow steel retainer ring. The hoops and the ring have some play within the WCM container to allow for mechanical tolerances and moved around every time the WCM was handled. This led to mysterious multi-GHz resonances that were never the same twice. Springs and RF gaskets were added to ensure that these parts would stay put.

Another intermittent several-GHz resonance was traced to the probe pins shown in Fig. 4. The pins have split tips designed to engage with some spring force in their sockets in the edge of the vacuum chamber across the gap. Sometimes, one of the prongs wouldn't touch the socket. From an EM point of view, the free prong is a little antenna resonating at a frequency where its length is $\frac{1}{4}\lambda$, at around 4 GHz. The problem was solved simply by splaying the prongs a little.

Both time domain and frequency domain reflectometry on the WCM output ports were indispensable to detect such problems.

PERFORMANCE MEASUREMENTS

Figure 11 shows the measured risetimes on individual ports. Since the ports closer to the centre of the beam pipe collect charge over a smaller section of the circumference, the signal rises much faster than for the ports farther away.
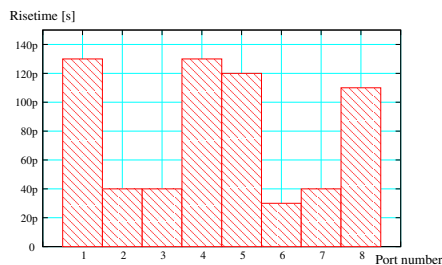
Figure 11: Risetimes measured on individual ports.

The final step response output signal, Fig. 12, has a risetime of 60 ps. The nicks near 13 ns and 17 ns are reflections from the end of the beam simulation rod and would not exist for real beams.

APPLICATION RESULTS

In the PS, the WCMs deliver signals for three main applications: low-level RF feedback, beam shape measurement and longitudinal phase space tomography (Fig: 13) [4]. The Tomoscope is an intensively used diagnostic tool in the PS
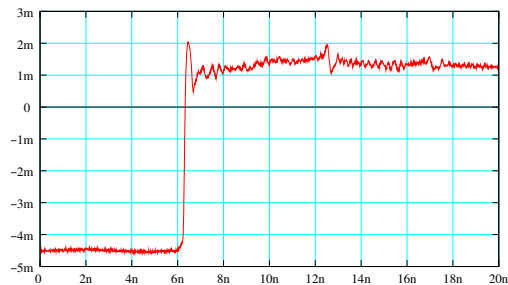
Figure 12: Overall combined output signal has a 60 ps step response risetime.

control room and the better signal quality and greater bandwidth of these WCMs have significantly improved the clarity of the tomograms.
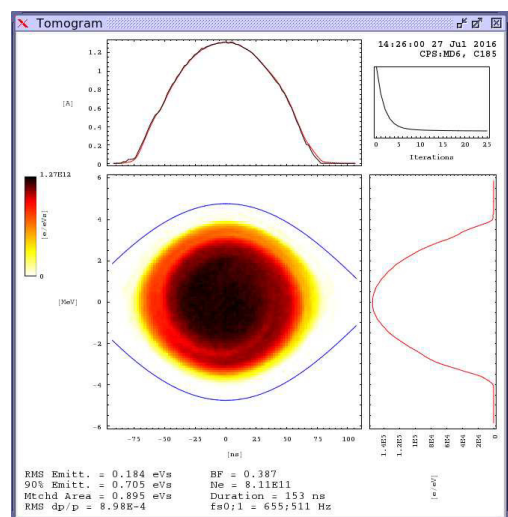
Figure 13: A longitudinal phase space tomogram of a proton bunch in the PS.

ACKNOWLEDGEMENTS

REFERENCES

[1] T.P.R. Linnecar, "The high frequency longitudinal and transverse pick-ups used in the SPS", CERN-SPS-ARF-78-17, CERN, Geneva, Switzerland.

[2] J. Durand, "Combining wideband signals from a wall current monitor", PS-LP-Note-94-14-Tech, CERN, Geneva, Switzerland.

[3] P. Odier, "A new wide band wall current monitor", CERN-AB-2003-063-BDI, CERN, Geneva, Switzerland.

[4] S. Hancock, P. Knaus, M. Lindroos, "Tomographic Measurements of Longitudinal Phase Space Density", CERN-PS-98-030-RF, CERN, Geneva, Switzerland.